Thermochimica Acta, 70 (1983) 291–302
Elsevier Science Publishers B.V., Amsterdam – Printed in The Netherlands

KINETIC INVESTIGATION OF THE SORPTION OF WATER BY BARIUM CHLORIDE MONOHYDRATE

JAN ANDERSSON, MICHEL AZOULAY and JOAN DE PABLO

Department of Physical Chemistry, The Royal Institute of Technology, S-100 44 Stockholm 70 (Sweden)

(Received 1 June 1983)

ABSTRACT

Using thermogravimetry under controlled water vapour pressure, the kinetics for the rehydration reaction

$$BaCl_2 \cdot H_2O(s) + H_2O(g) \rightarrow BaCl_2 \cdot 2\,H_2O(s)$$

was investigated as a function of various parameters of relevance in chemical heat pumps, i.e. the number of cycles, storage time, extent of dehydration, and particle size. The effect of cycling is interpreted in terms of a fragmentation process, as confirmed by scanning electron microscopy studies. Reaction rate isotherms were determined at four different temperatures (34.5, 40.3, 44.5 and 50.5°C), in the pressure range 18–66 torr. An inhibition pressure domain is observed. This effect is assumed to result from the formation of capillary condensed water. The presence of adsorbed water is clearly evidenced by wide-line NMR measurements.

INTRODUCTION

In recent years, much interest has been focussed on thermochemical reactions as a means of storing energy from intermittent sources, e.g. solar energy, waste heat and off-peak electrical energy [1,2]. In particular, a lot of effort has been devoted to the study of reversible desorption/sorption processes involving solid–gas reactions, e.g. of the type

$$AB(s) \rightleftarrows A(s) + B(g)$$

Thermochemical energy storage based on solid–gas reactions, where the gas can be condensed or bound (physically or chemically), has major advantages over classical storage methods: (i) a high storage density with respect to both weight and volume, and (ii) no need of thermal insulation since reaction products are separated. Moreover, desorption/sorption processes can be conveniently created using a heat pump in which the stored energy is, whenever needed, progressively released while the exothermic sorption process takes place. Thus, chemical systems such as the salt hydrates [3], methanolates [4], and ammoniates [5] have found their way into practical applications.

0040-6031/83/$03.00

The merits of chemical heat pump devices have been extensively discussed from various thermodynamic points of view for different configurations [6–8]. Much less attention has, however, been paid to the dynamic limitations that are inherent in the chemical systems and, thus, liable to reduce the suitability of the sorption process under consideration. A survey of the literature indicates that sorption kinetics is a poorly investigated topic. Hence, whereas a great amount of work has been devoted to various dynamic features of the dehydration reaction of the salt hydrates [9], only a few studies dealing with their rehydration kinetics have been reported [10–17]. It is increasingly recognized that more basic knowledge is required for a more direct application of chemical heat pumps. Particularly unsatisfactory is the situation prevailing for salt hydrates, the use of which has hitherto been severely limited.

As a first step in our work aimed at establishing the dynamic criteria for salt hydrates with regard to their suitability for chemical heat pumping, we decided to investigate the sorption kinetics for the reaction

$$BaCl_2 \cdot 2\ H_2O(s) \rightleftarrows BaCl_2 \cdot H_2O(s) + H_2O(g) \quad (1)$$

The present work is thus concerned with the dependency of rehydration rates on various operating parameters, e.g. the number of cycles, water vapour pressure, cold sink temperature, storage time, and the extent of dehydration. Reaction (1) was selected since it has been thoroughly investigated from various points of view. Reliable equilibrium data for this reaction are available in the literature [18,19]. The reaction was found to be to a large extent reversible [20]. Furthermore, the kinetics and the topotactic structural transformation associated with the dehydration process are well known [21–25].

The work reported in this paper involved the use of thermogravimetry, scanning electron microscopy and NMR spectroscopy.

EXPERIMENTAL

Materials

Crystalline $BaCl_2 \cdot 2\ H_2O$ (Merck p.a.) powders were classified by sieving and two different fractions were used: 63–80 μm and 100–125 μm. The compound was crystallographically identified as $BaCl_2 \cdot 2\ H_2O$ and used without further purification (see Results).

Experimental procedure

Desorption and sorption studies were performed mainly by means of thermogravimetry under controlled water vapour pressure according to the

cold point method [25]. The instrumental set-up is well suited for kinetic experiments in both isothermal and temperature scanning modes. In the isothermal runs the reaction was initiated by means of a pressure jump, which was performed by switching from one evaporator to another which was kept at a different temperature. The pressure corresponding to this temperature is denoted p_c, while the oven constraint temperature is termed T_c. Prior to a kinetic run the device was evacuated.

Throughout this study, unless otherwise stated, only those samples subjected to several dehydration–rehydration cycles (> 3) were used, and the isothermal dehydrations were performed at $p_c = 6$ torr, $T_c = 44.5°C$. The sample weight was about 40 mg which roughly corresponded to a monolayer. X-Ray diffractometry was employed for phase analysis of the products formed.

Instrumentation

The thermogravimetric equipment used, which consists of a McBain quartz spring balance, is described elsewhere [26]. With this instrumentation both weight and temperature changes were continuously recorded [27,28]. The temperature was indirectly measured by a thermocouple connected to a twin sample located close to the suspended sample pan.

X-Ray diffractograms were taken by means of a focussing Guinier camera.

^1H FT-NMR spectra were recorded at 90 MHz using a Bruker CXP 100. An evaporator was connected to the NMR tube to control the water vapour pressure. Microstructural studies were carried out using either an ISI or a Jeol 545 scanning electron microscope.

RESULTS

Kinetic studies by thermogravimetry

Measurements of progress curves under isobaric conditions—influence of the operating parameters

Fresh $BaCl_2 \cdot 2\ H_2O$ was taken for cycling experiments, which were conducted at $p_c = 6$ torr, $T_c = 44.5°C$ and 44.8 torr, 44.5°C for dehydrations and rehydrations, respectively. It was found that the dehydration and rehydration reaction rates increase substantially to attain a limiting value after three cycles as shown in Fig. 1. Moreover, the reactions appear to be completely reversible between the stoichiometric compositions corresponding to the mono- and dihydrates.

The delay time t_d between a complete dehydration ($> 99\%$) and rehydration was observed to affect the rehydration kinetics at 48.5 torr, 44.5°C, as displayed by the progress curves of Fig. 2. It is noteworthy that as the delay

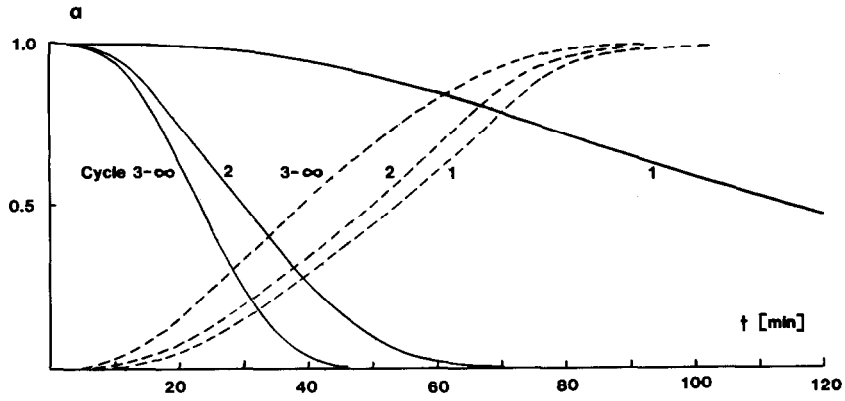

Fig. 1. Dehydration and rehydration progress curves during successive cycles of the reaction $BaCl_2 \cdot H_2O(s) + H_2O(g) \rightleftarrows BaCl_2 \cdot 2\,H_2O(s)$

Dehydrations and rehydrations were always achieved at $p_c = 6$ torr, $T_c = 44.5°C$ and 44.8 torr, 44.5°C, respectively. Particle size 100–125 μm. (Zero delay time between successive cyclings.)

time is increased the induction period increases, while the reaction rate decreases.

For a given dehydration–rehydration cycle partial dehydration leads to a sorption progress curve showing no induction period and also an increasing reaction rate. This result is illustrated in Fig. 2 for 90% dehydration.

In the temperature scanning mode at constant pressure, a strong hysteresis becomes noticeable in the dehydration–rehydration cycle (see Fig. 3). However, no attempt was made to analyze a thermogram in quantitative terms.

In following the sample temperature during a rehydration run, two different temperature peaks corresponding to a fast and a slow increase were

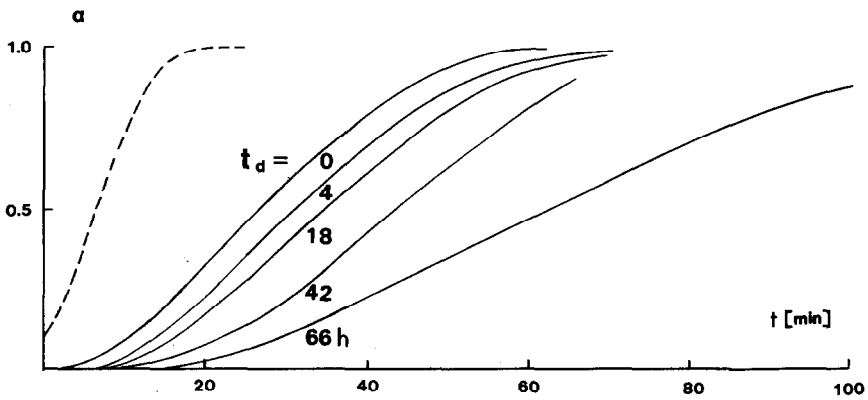

Fig. 2. Rehydration curves for reaction (1) at (48.5 torr, 44.5°C). Full curves refer to the rehydration following a complete dehydration (< 99%), after different delay times. The dashed curve was recorded immediately after a 90% dehydration.

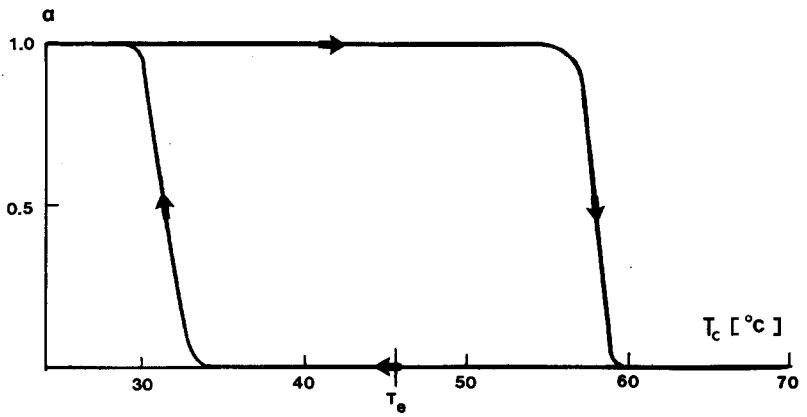

Fig. 3. A typical thermogram for a dehydration/rehydration cycle of a cycled sample under isobaric conditions ($p_c = 25$ torr). Temperature range, 30–60°C; scanning rate, 3°C h^{-1}, particle size, 100–125 μm. $T_e = 45.7$°C refers to the equilibrium temperature from ref. 18.

detected. The fast increase was observed immediately after the pressure jump. This effect was enhanced at higher pressures p_c at constant T_c. After temperature equilibration the reverse was noticed for negative pressure jumps. In both cases slow exponential relaxation towards the initial sample temperature was recorded. The fast temperature increase was also found to be suppressed when the delay time was increased. The slower temperature increase was associated with a relatively large water uptake as indicated by the simultaneous weight change.

In order to gain further insight into the nature of this thermal phenomenon, more experimental evidence was collected by recording wide-line proton NMR spectra. These measurements were carried out under conditions similar to those in the TG experiments. However, a larger amount of substance had to be used. The NMR spectra consisted of the doublet corresponding to the well-known "powder spectrum" [29].

When the water vapour was let into the NMR tube the sorption of water resulted in a new but comparatively narrow peak characterizing loosely bound water. This resonance can thus be attributed to water adsorbed at the surface layers of the sample. It should be mentioned that the differences in the powder spectra corresponding to $BaCl_2 \cdot H_2O$ and $BaCl_2 \cdot 2\,H_2O$ were minor.

Characteristics of the reaction rate isotherm

The influence of the pressure p_c *and the particle size* d_p. For a given temperature T_c, progress curves were measured at various pressures p_c and particle sizes d_p. The reaction rates v_{max} $[= (d\alpha/dT)_{max}]$ were inferred from their inflexion points. The values obtained are plotted in Fig. 4. It is interesting that the reaction rate isotherms do not intersect the pressure axis

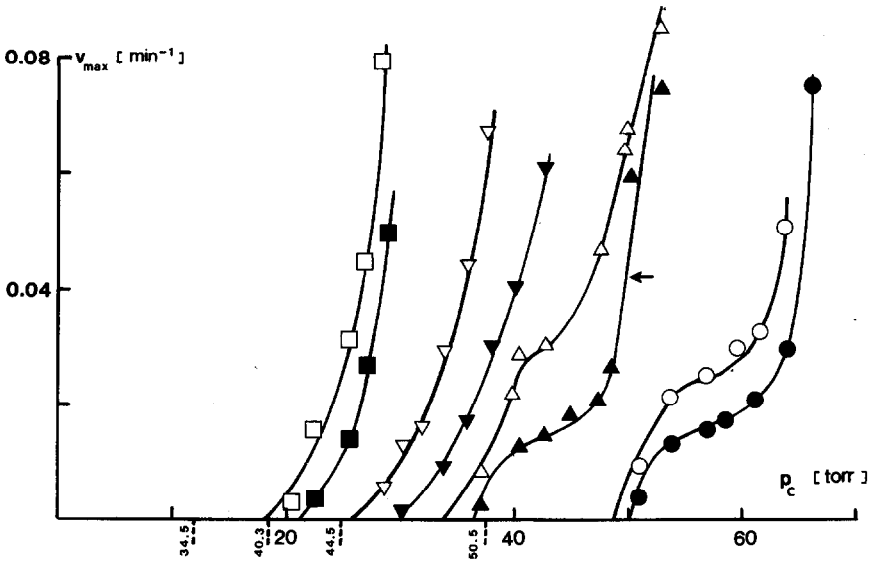

Fig. 4. Reaction rate isotherms vs. pressure for reaction (1) at four different temperatures T_c and two different particle sizes d_p: $T_c = 34.5°C$ (□,■); $T_c = 40.3°C$ (▽,▼); $T_c = 44.5°C$ (△,▲); $T_c = 50.5°C$ (○,●). Open and filled symbols refer to $d_p = 60–83$ μm and $d_p = 100–125$ μm, respectively.

at the equilibrium pressures p_e [18] which are added in the plot; in fact the observed deviations are about 10 torr. It should be mentioned that similar results have been obtained previously for ammoniates [30]. Another interesting feature is that at higher temperatures the reaction rate isotherms contain a plateau appearing at an intermediate pressure range before the rate increases abruptly. Finally, decreasing the particle size leads to a higher reaction rate.

The influence of partial dehydration. For the purpose of comparison, the v_{max} values at various pressures for 50% dehydration are given in Table 1. These values have been obtained at $T_c = 44.5°C$, $d_p = 100–125$ μm and thus should be compared to the corresponding points for the 100% curve (see the curve indicated by an arrow in Fig. 4).

TABLE 1

Rehydration reaction rates v_{max} at $T_c = 44.5°C$ and at various pressures for 50% dehydration

p (torr)	$v_{max} \times 10^3$ (min^{-1})
30.3	1 (0) [a]
33.6	7 (0)
38.0	12 (6)
45.0	40 (19)

[a] v_{max} values in parentheses refer to interpolated values from the curve in Fig. 4 indicated by an arrow (100% dehydration).

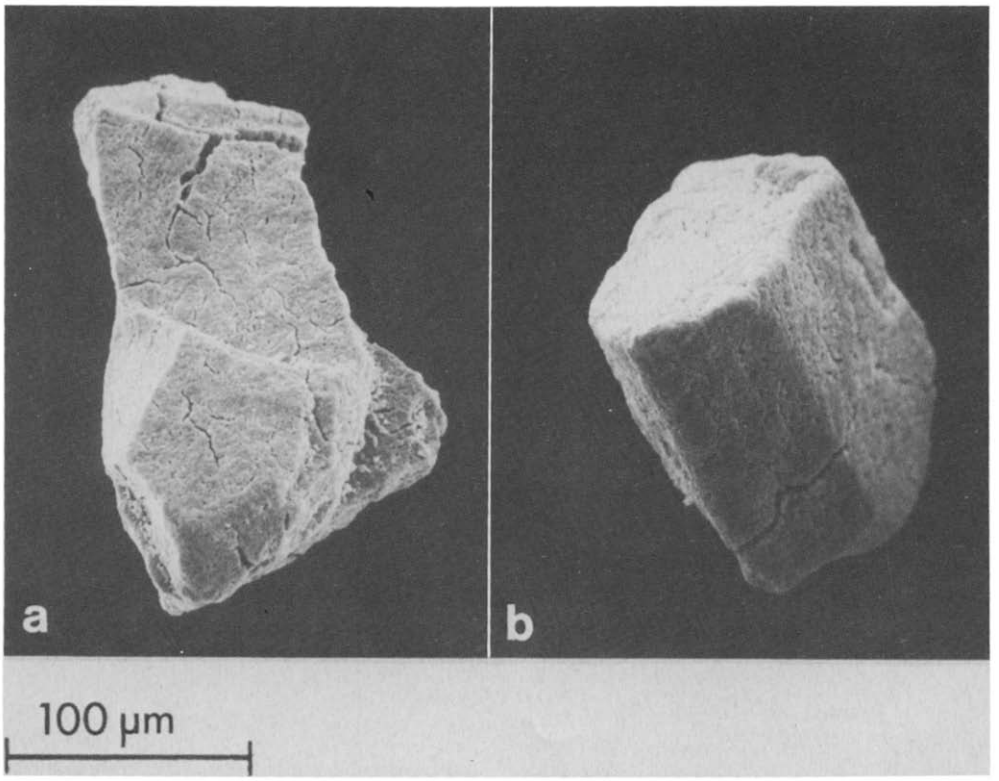

Fig. 5. Scanning electron micrograph of $BaCl_2$ particles (cycled specimens) using the emissive mode (400×): (a) after dehydration; (b) after rehydration.

Phase analysis of the reaction products

Following several dehydration–rehydration cycles both dehydrated and rehydrated products were crystallographically characterized by their X-ray powder diffractograms.

Rehydration gives back the original diffraction pattern associated with the fresh $BaCl_2 \cdot 2\ H_2O$ [31], thus evidencing a reversible structure transformation. The cycled samples obtained upon dehydration as inferred from their powder diffractograms had *d* spacings comparing well with those previously reported for $BaCl_2 \cdot H_2O$ [32]. However, the reflections included in these diffractograms appear somewhat broader than those relating to the dihydrate.

Microstructural analysis using scanning electron microscopy (SEM)

In order to reveal possible texture changes proceeding at the particle level which could account for the kinetic behaviour observed during cycling,

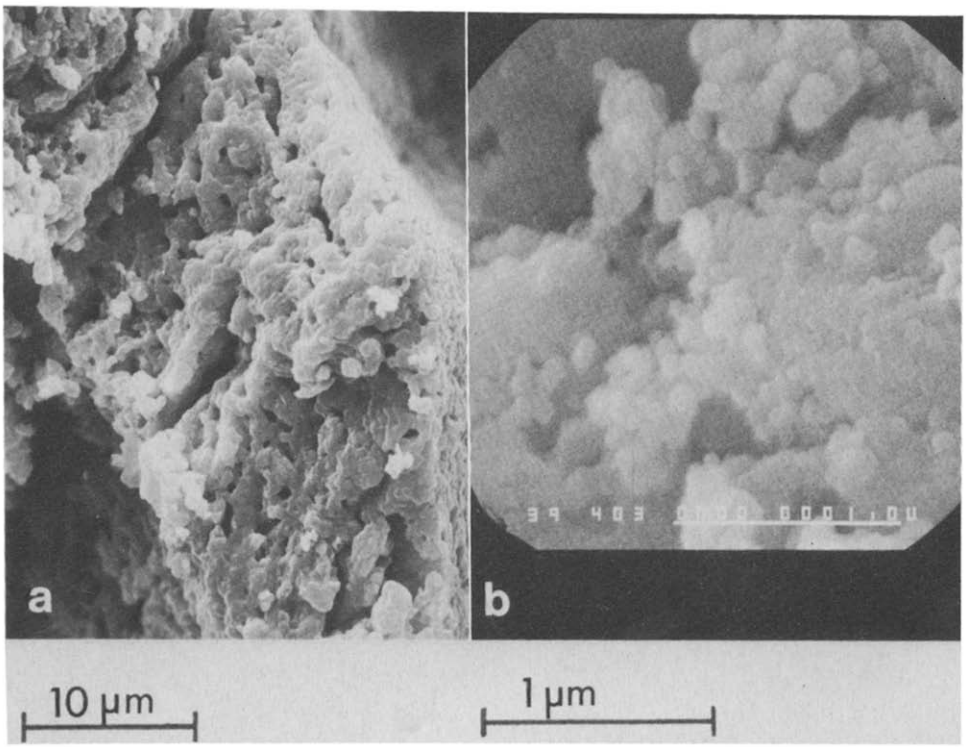

Fig. 6. Scanning electron micrographs showing the internal structure of (a) a sectioned $BaCl_2 \cdot 2\,H_2O$ particle (3000×); (b) a sectioned $BaCl_2 \cdot H_2O$ particle (40000×).

scanning electron microscopic examinations of dehydrated and rehydrated cycled samples were made in the magnification range 400–40000X. Figure 5 contains microphotographs of $BaCl_2 \cdot H_2O$ and $BaCl_2 \cdot 2\,H_2O$ particles at the same magnification. Both the particles show substantial fracturation which proceeds across the particle (cf. Fig. 6a). It should be noted that the external shape of the particles seems to remain unchanged. The micrographs in Fig. 6 showing particle cross-sections taken at a relatively high degree of magnification reveal the internal structure of cycled $BaCl_2 \cdot 2\,H_2O$ (Fig. 6a) and $BaCl_2 \cdot H_2O$ (Fig. 6b). Figure 6a shows a three-dimensional network of cracks and pores. A layer arrangement of subparticles can also be observed. Obviously the texture properties of these particles ought to facilitate the water vapour transport during the course of the reaction. In the microphotograph of Fig. 6b (40000×), subparticles as small as ~800 Å can be detected.

DISCUSSION

From our temperature scanning measurements (cf. Fig. 3), the equilibrium temperature, at $p_e = 25$ torr, of reaction (1) can be roughly estimated as

45°C. This value is in fair agreement with those obtained in two previous studies [18,19]. The equilibrium data obtained from static measurements [18] considered in this work are displayed in Fig. 7.

For solid–gas surface reactions the rate is governed by factors such as the mass transfer of the gaseous species into the reaction centres, the total surface area, the average surface density of defects, and the heat transfer between the solid and the gas phases.

Assuming that cycling leads to a fragmentation process, the first three factors would, under similar conditions of heat transfer, act in the same direction, i.e. they increase the reaction rate. This readily provides an interpretation of our kinetic data relating to dehydration and rehydration (cf. above). This fragmentation process leads to the limiting condition which is achieved after the third cycle. It is likely that surface defects are created during fragmentation at the reaction interface as a result of mechanical stress owing to the molar volume changes (ca. 12%). The latter forms the basis of the cracking, as has already been noted in a previous dehydration study [22] and which is confirmed by our scanning electron microscopic observation (see Fig. 5).

More evidence which seems to support the fragmentation process is the observation of units corresponding to 800 Å in diameter, believed to constitute the limiting size of the subparticles formed. The porous particles formed in this way should facilitate the transport of water vapour to the reacting surface. The possibility of the occurrence of an effusion process in

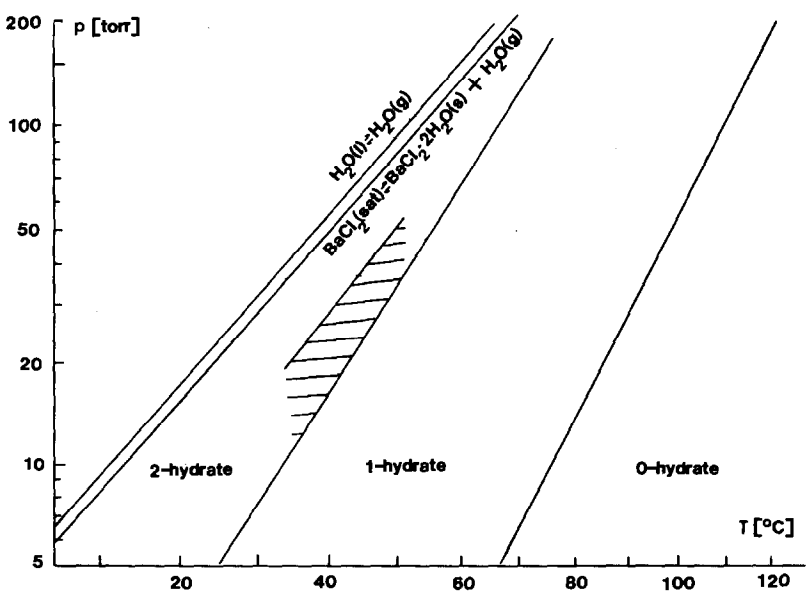

Fig. 7. Pressure–temperature diagram showing the deceleration domain (hatched area) for the rehydration process. Equilibrium data are taken from ref. 18.

the working pressure range 20–70 torr cannot be discarded on the basis of rough estimates, since the calculated mean free path is of the same order of magnitude as the observed pore diameter (ca. 1 μm). However, this step cannot be considered as rate-limiting, because the calculated values are higher than those observed experimentally by three orders of magnitude.

The dependence of the rehydration kinetics on storage time can readily be accounted for by the ageing of the dehydrated solid. It is well known that surface defects disappear in such processes. This is consistent with the observation that high reaction rates are accompanied by a short induction period (see Fig. 2).

For the above reasons it is understandable that the induction phase is absent in the rehydration curve after partial dehydration since numerous defects are likely to be present at the interface between the two hydrates. This experimental finding can also be attributed to the presence of the new phase, which plays the role of a template for the structure transformation.

The observation of thermal and mass (at least 0.2%) changes, together with the NMR finding, gives, as has already been mentioned, strong support for the hypothesis that a water layer is formed during the course of the reaction.

The disappearance of defects which can otherwise be evidenced in the kinetic data collected in Table 1 is hardly understandable without assuming a thick water layer. Such a layer could provide an efficient means of cancelling surface defects. These two series of measurements exhibit large discrepancies although 50% of both phases is present in both cases. The lower v_{max} values shown in parentheses in Table 1 are due to a higher exposure time to the water.

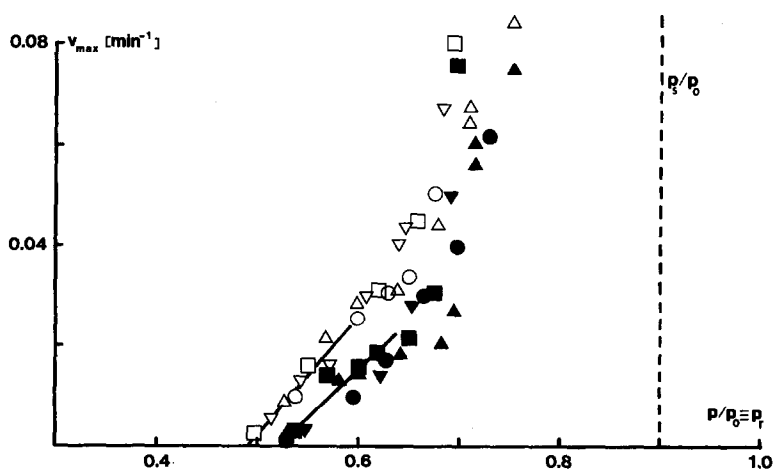

Fig. 8. Maximum reaction rate vs. relative pressure (p_r) for the rehydration reaction. Particle size, cf. Fig. 4. p_s and p_0 refer to the vapour pressures of a saturated barium chloride solution (with respect to $BaCl_2 \cdot 2\,H_2O$) and of pure water (saturation), respectively.

The adsorbed water molecules might possibly, as a consequence of the internal structure of the particles, be related to water films embedded between adjacent subparticle layers and formed via capillary condensation. In order to test the validity of this assumption the v_{max} values at the four different temperatures are displayed as a function of relative pressures ($p_r = p/p_0$) in Fig. 8. This plot shows that close to equilibrium pressure the v_{max} values tend to form a straight line independent of the temperature. The fast increase in the reaction rate with increases in the relative pressure suggests that capillary condensation could actually be the kinetic controlling step for rehydration. This also provides a straightforward explanation of the inhibition effect shown by the reaction rate isotherm of Fig. 4, since a reaction could not be initiated at relative pressure values below ~ 0.5. In other words, the inhibition domain appearing in the pressure–temperature diagram in Fig. 7, in which capillary condensation is absent, applies for the actual rehydration.

For all the reaction rate curves presented in Fig. 4, and at the same T_c and p_c, the v_{max} values are higher for the lower particle sizes. Under stationary heat-flow conditions during the reaction, the particle temperature should become higher for larger particles. In this case, the stationary temperature gets closer to the equilibrium temperature corresponding to p_c, and therefore is expected to slow down the reaction.

At the present stage of this work, the appearance of the plateau observed at higher temperatures (44.5 and 50.5°C) is not fully understood. Tentatively we suggest that the explanation can be sought in a more pronounced ageing behaviour at these higher temperatures.

ACKNOWLEDGEMENTS

This work was supported by the Swedish Natural Science Research Council under Contract No. E-EG 2741-112. The authors are indebted to Professor G. Wettermark for his continuous interest and encouragement in this work. We gratefully acknowledge Professor G. Bertrand for valuable discussions.

REFERENCES

1 G. Wettermark (Ed.), Proceedings from the International Seminar on Thermochemical Energy Storage, Stockholm, 1980, Swedish Council for Building Research.
2 H. Bjurström and W. Raldow, Int. J. Energy Res., 5 (1981) 43.
3 E.A. Brunberg, The Tepidus Storage System, German–Swedish Workshop on Thermochemical Energy Storage and Absorption Heat Pump Technology, Stockholm, 1980.
4 P.O'D. Offenhartz, J. Sol. Energy Sci. Eng., 102 (1980) 59.
5 S. Elberg and P. Mathonnet, Rev. Phys. Appl., 17 (1982) 585.

6 P.O'D. Offenhartz, Chemical Methods of Storing Energy, Jt. Conf. Amer. Can. Sect. ISES, Vol. 8, 48, Winnipeg, 1976.
7 W.M. Raldow and W.E. Wentworth, Sol. Energy, 23 (1979) 75.
8 H. Stymne, in G. Wettermark (Ed.), Proceedings from the International Seminar on Thermochemical Energy Storage, Stockholm, 1980, Swedish Council for Building Research, p. 65.
9 M.E. Brown, D. Dollimore and A.K. Galwey, in C.H. Bamford and C.F.H. Tipper (Eds.), Comprehensive Chemical Kinetics, Vol. 22, Elsevier, Amsterdam, 1980, p. 122.
10 A. Bielanski and F.C. Tompkins, Trans. Faraday Soc., 46 (1950) 1072.
11 R.M. Dell and S.W. Weller, Trans. Faraday Soc., 55, (12) (1959) 2203.
12 P. Barret and R. Thiard, C.R. Acad. Sci. Paris, 260 (1965) 2823.
13 N. Gérard, G. Watelle-Marion and A. Thrierr-Sorel, Bull. Soc. Chim. Fr., 5 (1967) 1788.
14 M. Trollier and B. Guilhot, C.R. Acad. Sci. Paris, Ser. C, 281 (1975) 27.
15 M. Trollier and B. Guilhot, Bull. Soc. Chim. Fr., (1977) 1.
16 B. Beden, A. Cointot, M.J. Croissant and G. Valensi, Kinetics in Heterogeneous Chemical Systems, Elsevier, Amsterdam, 1975.
17 S. El and D. Hamad, Thermochim. Acta, 17 (1976) 85.
18 E.M. Collins and A.W.C. Menzies, J. Phys. Chem., 40 (1936) 379.
19 L.G. Berg and V.P. Kovyrzina, Z. Neorg. Chim., 9 (1) (1964) 14.
20 E. Buzágh-Gere, S. Gál and J. Simon, in H.G. Wiedermann (Ed.), Thermal Analysis, Proceedings Third ICTA, Davos, 1971.
21 G.G.T. Guarini and R. Spinicci, J. Therm. Anal., 4 (1972) 435.
22 R.K. Osterheld and P.R. Bloom, J. Phys. Chem., 82 (1978) 1591.
23 H. Tanaka and K. Maeda, Thermochim. Acta, 51 (1981) 97.
24 H. Tanaka, Thermochim. Acta, 52 (1982) 1.
25 A. Tiselius and S. Brohult, Z. Phys. Chem., Abt. A, 168 (1935) 248.
26 F. Lavanant, Thesis, Dijon, 1963.
27 P. Barret, Bull. Soc. Chim. Fr. Mem., 58 (1958) 376.
28 M. Lallemant, Thesis, Dijon, 1974.
29 E.R. Andrew, Nuclear Magnetic Resonance, University Press, Cambridge, 1955.
30 R. de Hartoulari, L.-C. Dufor and P. Barret, Colloq. Int. CNRS, Thermochim., No. 201 (1973).
31 ASTM, $BaCl_2 \cdot 2\,H_2O$, Card No. 25-1135.
32 ASTM, $BaCl_2 \cdot H_2O$, Card No. 1-821.